Weak-constraint inverse modeling using HYSPLIT Lagrangian dispersion model and Cross Appalachian Tracer Experiment (CAPTEX) observations – Effect of including model uncertainties on source term estimation

Tianfeng Chai[*,a,b], Ariel Stein[a], Fong Ngan[a,b]

[a] *NOAA Air Resources Laboratory (ARL), NOAA Center for Weather and Climate Prediction, 5830 University Research Court, College Park, MD 20740, USA*
[b] *Cooperative Institute for Climate and Satellites, University of Maryland, College Park, MD 20740, USA*

Abstract

The Cross Appalachian Tracer Experiment (CAPTEX) data collected from six controlled releases are used to quantitatively evaluate a HYSPLIT inverse system which is based on variational data assimilation and a Lagrangian dispersion transfer coefficient matrix (TCM). Inverse modeling tests with various observational uncertainties show that using concentration differences results in severe underestimation while using logarithm concentrations differences results in overestimation of the release rate. The introduction of model uncertainty terms improves results for both choices of the metric variables in the cost function. To avoid spurious minimal source term solutions when using logarithm concentrations as metric variables the cost function is normalized by the weighting term sum. Such normalization is effective in eliminating the spurious solutions and it also helps to improve release estimates for both choices of the metric variables. The tests with many combinations of uncertainty parameters show that having logarithm concentrations as metric variables generally yield better results than those having concentrations as metric variables and the estimates are quite robust for a reasonable range of model uncertainty parameters. Such conclusion is further confirmed with nine ensemble runs in which meteorological fields were generated with

[*] Corresponding author
Email address: `Tianfeng.Chai@noaa.gov` (Tianfeng Chai)

varying planetary boundary layer (PBL) schemes using a different version of the Weather Research and Forecasting (WRF) Model. In addition, the emission estimates using the median transfer coefficients of the nine TCMs are compared with the medians of the nine estimates using the nine simulations individually for various combinations of model uncertainty parameters. It is found that the two approaches give similar results for both choices of metric variables with 12 model uncertainty parameter combinations. The relative differences are not greater than 3.1% for logarithm concentration metric variable and not greater than 10.8% for concentration metric variables. With a fixed set of observational and model uncertainty parameters, the inverse method with logarithm concentration as metric variable is then applied to other releases and the largest relative error is 53.3% among the six releases. The system is later tested for its capability to locate a single source location as well as its source strength. The location and strength that result in the best match between the predicted and the observed concentrations are considered as the best estimates. The estimated location is close to the actual release site for release 2 of which the HYSPLIT has the best performance with the exact source terms. The estimated release rates are mostly not as good as the cases with the exact release site assumed known, but they are within a factor of 3 for all releases.

Key words: HYSPLIT, Lagrangian dispersion model, source term estimation, transfer coefficient matrix (TCM), ensemble

---

1. Introduction

The transport and dispersion of gaseous and particulate pollutants are often simulated to generate pollution forecasts for emergency responses or produce comprehensive analyzes of the past for better understanding of the particular events. Lagrangian particle dispersion models are particularly suited to provide plume products associated with emergency response scenarios. However, the exact air pollutants source terms are rarely provided in most scenarios. For instance, the smoke forecasts over the continental U.S. operated by the National Oceanic and Atmospheric Administration (NOAA) using the HYSPLIT model [16, 44] in support of the National Air Quality Forecast Capability (NAQFC) relies on the outdated fuel loadings data and a series of assumptions related to smoke release heights and strength approximation [40].

Observed concentration, deposition, or other functions of the atmospheric pollutants such as aerosol optical thickness measured by satellite instruments can be used to estimate some combination of source location, strength, and temporal evolution using various source term estimation (STE) methods [3, 26]. Among the applications, the recent Fukushima Dai-ichi Nuclear Power Plant accidents saw the most implementations of the STE methods to estimate the radionuclide releases. The STE methods range from simple comparisons between model outputs and measurements [e.g. 12, 29, 46, 24, 30, 36, 28, 1] to those sophisticated ones using various dispersion models and inverse modeling schemes [e.g. 45, 53, 41, 52, 10]. Another active field for STE applications is the estimation of the volcanic ash emissions. Many attempts have been made for several major volcano eruptions [49, 39, 50, 51, 9].

While there are many STE methods applied to reconstruct the emission terms, it is still a state of art. Two popular advanced inverse modeling approaches are cost-function-based optimization methods and those based on Bayesian inference. For most applications, it is very difficult to effectively evaluate the results without knowing the actual sources. Chai et al. [10] generated pseudo observations using the same dispersion model in its initial inverse experiment tests, which are often called "twin experiments". Such tests can have observation errors realistically added [e.g. 10], but it is non-trivial to represent the model errors incurred by other model parameters such as the uncertainties of the meteorological field. One way to objectively evaluate the inverse modeling results is comparing the predictions with the estimated source terms against the independent observations or withheld data. However, such indirect comparisons still cannot provide quantitative error statistics for the source terms.

There are tracer experiments conducted to study the atmospheric transport and dispersion where controlled releases were well-quantified and comprehensive measurements were made subsequently over an extended area [e.g. 15, 48]. Such data sets have been extensively used to evaluate the dispersion models [e.g. 19, 22, 23]. The known source terms can also provide a unique opportunity to evaluate the estimated emission sources by the STE methods. For instance, the European Tracer Experiment (ETEX) data set was used to study the STE methods based on the principle of maximum entropy and a least squares cost function [4, 5, 6]. Singh and Rani [42] and Singh et al. [43] used measurements from a recent dispersion experiment (Fusion Field Trials 2007) data to evaluate a least-squares technique for identification of a point release. However, such formal evaluation of the STE methods is very

limited.

HYSPLIT inverse system based on 4D-Var data assimilation and a transfer coefficient matrix (TCM) was developed and applied to estimate cesium-137 source from the Fukushima nuclear accident using air concentration measurements [10]. The system was further developed to solve the effective volcanic ash release rates as a function of time and height by assimilating satellite mass loadings and ash cloud top heights. Chai et al. [9] tested and evaluated the system using the Kasatochi eruption in 2008 as an example. In this study, the Cross Appalachian Tracer Experiment (CAPTEX) tracer experiment data are used to evaluate a HYSPLIT inverse modeling system in its ability to estimate the source strength and its release location. The paper is organized as follows. Section 2 describes the CAPTEX experiment, HYSPLIT model configuration, and the source term inversion method. Section 3 presents emission inversion results and a summary is given in Section 4.

2. Method

2.1. CAPTEX experiment

The CAPTEX experiment consisted of seven near-surface releases of the inert tracer perfluro-monomethylcyclohexane (PMCH) from Dayton, Ohio, U.S. and Sudbury, Ontario, Canada during September and October 1983 [14]. Table 1 lists the locations, time, released tracer amounts, and measurement counts of all seven releases. Samples were collected at 84 different measurement sites distributed from 300 to 1100 km downwind of the emission source, as either 3- or 6-hour averages up to 60 hours after each release. Figure 1 shows the distribution of two source locations and all measurement sites during the CAPTEX period. Since there were few measurements above twice background values for release 6 as the plume being very narrow, it will be excluded from the testing as in the earlier studies using CAPTEX data [e.g. 23, 35].

2.2. HYSPLIT

In this study, the tracer transport and dispersion are modeled using the HYSPLIT model in its particle mode in which three-dimensional Lagrangian particles released from the source location passively follow the wind field [16, 17, 44]. A particle release rate of 50,000 per hour is used for all calculations. Random velocity components based on local stability conditions are added to the mean advection velocity in the three wind component directions. The

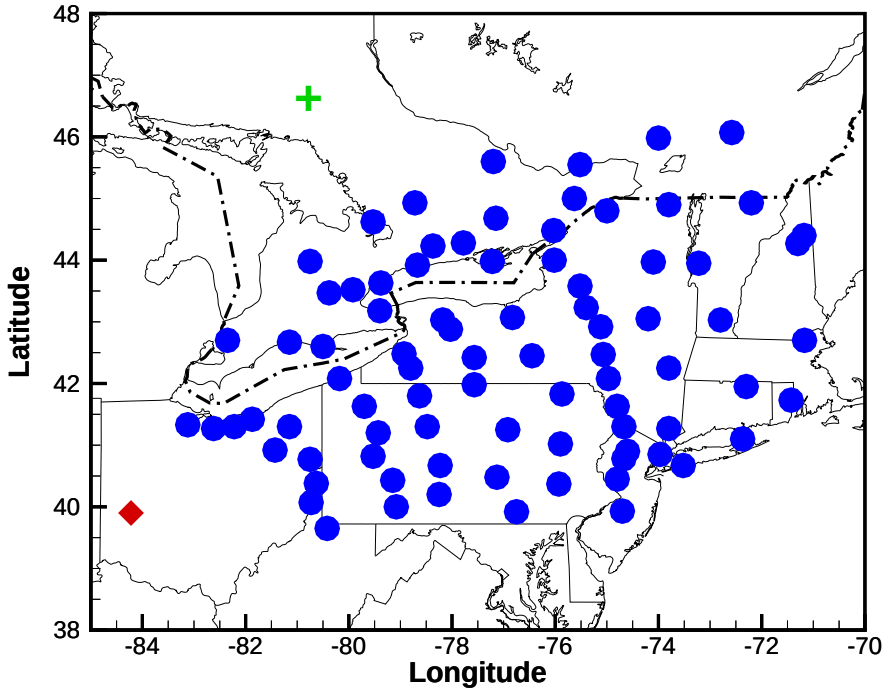

Figure 1: Distribution of two CAPTEX source locations, Dayton, Ohio, U.S. shown as a red diamond, and Sudbury, Ontario, Canada shown as a green cross, and the 84 measurement sites.

Table 1: The location, time, released tracer amounts, and measurement counts (M_{obs}) of each CAPTEX release from Dayton, Ohio, U.S. and Sudbury, Ontario, Canada during September and October 1983.

#	Site (latitude, longitude)	Release time	Amount	M_{obs}
1	Dayton (39.80°, -84.05°)	1700-2000Z, Sep. 18, 1983	208 kg	395
2	Dayton (39.90°, -84.22°)	1705-2005Z, Sep. 25, 1983	201 kg	400
3	Dayton (39.90°, -84.22°)	1900-2200Z, Oct. 02, 1983	201 kg	404
4	Dayton (39.90°, -84.22°)	1600-1900Z, Oct. 14, 1983	199 kg	367
5	Sudbury (46.62°, -80.78°)	0345-0645Z, Oct. 26, 1983	180 kg	357
6	Dayton (39.90°, -84.22°)	1530-1600Z, Oct. 28, 1983	32 kg	-
7	Sudbury (46.62°, -80.78°)	0600-0900Z, Oct. 29, 1983	183 kg	358

meteorological data used to drive the HYSPLIT are identical to those time-averaged Advanced Research WRF model (ARW, version 3.2.1) simulation at 10-km resolution used by Hegarty et al. [23]. The 10-km run was nested inside a larger domain at 30-km resolution, over which the simulation was started using the North American Regional Reanalysis at 32-km [32]. In the WRF simulations, 3D grid nudging of winds was applied in the free troposphere and within the planetary boundary layer (PBL). There are 43 vertical layers with the lowest one being approximately 33 m thick. Tracer concentrations are computed over each grid cell by summing the mass of all particles in the cell and dividing the result by the cell's volume. In this study, the concentration grid cells have a 0.25^o resolution in both latitude and longitude directions and have a height of 100 m starting from surface.

To avoid running the HYSPLIT modeling repeatedly, a transfer coefficient matrix (TCM) is generated for each inverse modeling problem, similar to the previous HYSPLIT inverse modeling studies [10, 9]. As described in Draxler and Rolph [18], independent simulations are performed with a unit emission rate from each source location and pre-defined time segment. Each release scenario is simply a linear combination of the unit emission runs.

2.3. Emission Inversion

Similar to [10], the unknown releases can be solved by minimizing a cost functional that integrates the differences between model predictions and observations, deviations of the final solution from the first guess (*a priori*), as

well as other relevant information written into penalty terms [13]. For the current application, the cost functional $\mathcal{F}$ is defined as,

$$\begin{aligned}\mathcal{F} = \quad & \frac{1}{2}\sum_{i=1}^{M}\sum_{j=1}^{N}\frac{(q_{ij}-q_{ij}^{b})^2}{\sigma_{ij}^2} + \frac{1}{2}\sum_{m=1}^{M}\frac{(c_m^h - c_m^o)^2}{\epsilon_m^2} \\ + \quad & \frac{c_{sm}}{2}\cdot\sum_{i=2}^{N-1}[\frac{(q_{i-1,j}-q_{i-1,j}^{b}) - 2\cdot(q_{ij}-q_{ij}^{b}) + (q_{i+1,j}-q_{i+1,j}^{b})}{q_c}]^2 \quad (1)\end{aligned}$$

where q_{ij} is the discretized source term at hour i and location j for which an independent HYSPLIT simulation has been run and recorded in a TCM. q_{ij}^b is the first guess or *a priori* estimate and σ_{ij}^2 is the corresponding error variance. Note that all tracer sources in this study were at ground level and the release heights in the HYSPLIT were set as 10 m for all the following test cases. We also assume the uncertainties of the release at each time-location are independent of each other so that only the diagonal term of the typical *a priori* error variance σ_{ij}^2 appears in Equation 1. c^h and c^o denote HYSPLIT-predicted and measured concentrations, respectively. The observational errors ϵ_m^2 are assumed to be uncorrelated. The term "observational errors" does not limit ϵ_m^2 to include the observational uncertainties only. As the term ϵ_m^2 is essentially used to weight $(c_m^h - c_m^o)^2$ terms, the uncertainties of the model predictions and the representative errors should all be considered along with the observational uncertainties. This will be further discussed in Section 3.2. The last term is a smoothness penalty and it helps to make the modified minimization problem better conditioned [31]. q_c is a scale constant and may be combined with c_{sm} to adjust the smoothness term. In this study, the smoothness penalty is turned off by setting c_{sm} as zero. A large-scale bound-constrained limited-memory quasi-Newton code, L-BFGS-B [54] is used to minimize the cost functional $\mathcal{F}$ defined in Equation 1 when multiple parameters need to be determined, but it is not needed here. As shown by Chai et al. [10], the control and metric variables can be changed to $ln(q_{ij})$ and $ln(c_m^h) - ln(c_m^o)$. Both choices of metric variable will be tested here.

3. Results

3.1. Recovering emission strength without model uncertainty

As an initial test, the exact release location and time are both assumed known and the only unknown variable left to be determined is the release rate, or the total release amount. For this type of one-dimensional problem, an optimal emission strength can be easily found without having to use sophisticated minimization routines. For instance, the $\mathcal{F}$ may be directly calculated for a number of emission strength values and the resulting $\mathcal{F} = \mathcal{F}(q)$ plot will reveal the optimal q strength that is associated with the minimal $\mathcal{F}$. Note that such an optimal solution not only depends on the chosen parameters in Equation 1, but also highly depends on the HYSPLIT model setup and the meteorological fields.

Both Hegarty et al. [23] and Ngan et al. [35] showed that the HYSPLIT dispersion model performed better for Release 2 than the other releases. Thus Release 2 is initially chosen to perform a series of sensitivity tests. Assuming no prior knowledge of the emission strength, the first guess is given as $q^b = 0$, and the $\sigma = 10^4 \ \ kg/hr$ is assumed. Sensitivity tests show that when q^b is changed to 100 kg/hr the emission strength estimates are nearly unchanged with the same or larger σ. Note that 3.4 fl/l has been subtracted from all CAPTEX measurements to remove background and "noise" in sampling where the ambient background concentration is constant at 3.0 fl/l [20]. At ground level, 1 fl/l is equivalent to 15.6 pg/m^3. Duplicate sample analyses showed that the majority data has a mean standard deviation estimated as 10.8% and contaminated samples may have standard deviation as large as 65% [20].

Firstly, the observational uncertainties are formulated to include a fractional component $f^o \times c^o$ and an additive part a^o. No model uncertainties are considered to contribute to ϵ. Table 2 lists the emission strength q that generates the minimal cost function for a series of f^o and a^o combinations, where f^o ranges from 10% to 50%, and a^o taking 10, 20, and 50 pg/m^3. All the emission strength values obtained are significantly lower than the actual release of 67 $\ \ kg/hr$. It shows that a larger f^o value tends to have a smaller q estimate, but a larger a^o results in a larger q. The significant underestimation of the release strength is caused by the implicit assumption of a perfect model when ϵ does not include the model uncertainties. Figure 2 shows the comparison between the predicted and measured concentrations when the actual release rate of 67 $\ \ kg/hr$ is applied. It shows that large discrepancies

still exist even when the exact releases are known and used in the simulation. For the measured zero concentrations, most of the predicted values are non-zero and the model predictions can be above 1000 pm/m^3. As $\epsilon_m = a^o$ for these zero concentrations, $\frac{(c_m^h - c_m^o)^2}{\epsilon_m^2}$ will dominate the cost function when a^o is not large enough. This explains that the underestimation is not as severe for a^o =50 pg/m^3 as that for a^o =10 pg/m^3. While ϵ do not change with f^o for the zero concentrations, smaller f^o values help increase the weighting of the terms $\frac{(c_m^h - c_m^o)^2}{\epsilon_m^2}$ associated with large measured concentrations. So, the estimated emission strength when $f^o = 10\%$ is better than when $f^o = 50\%$.

As stated in Chai et al. [10], the metric variable in Equation 1 can be changed to $ln(c)$, i.e. replacing $(c_m^h - c_m^o)$ with $ln(c_m^h) - ln(c_m^o)$. A constant 0.001 pg/m^3 is added to both c_m^h and c_m^o to allow the logarithm operation for zero concentrations. In such a case, $\epsilon_m^{ln(c)}$ can be calculated as

$$\epsilon_m^{ln(c)} = ln(1 + f^o + \frac{a^o}{c_m^o}) \tag{2}$$

Note that a constant small number 0.001 pg/m^3 is also added to c_m^o in the second term to avoid dividing by zero. The $\frac{a_m^o}{c_m^o}$ term in Equation 2 makes $\epsilon_m^{ln(c)}$ larger for measured low concentrations than those measured high concentrations, thus makes the measured zero concentrations have little effect in the final emission strength estimates. Table 3 shows that the emission strengths are overestimated, but are within a factor of 2 over the actual release of 67 kg/hr, for all f^o and a^o combinations. The similar trends of how q changes with f^o and a^o are also observed here, i.e., a larger a^o or a smaller f^o tends to have a larger q estimate.

Table 2: Emission strength of release 2 that minimizes $\mathcal{F}$ for different observational errors, defined as $\epsilon = f^o \times c^o + a^o$. Concentrations are used as the metric variables.

Emission (kg/hr)	a^o =10 pg/m^3	a^o =20 pg/m^3	a^o =50 pg/m^3
$f^o = 10\%$	7.1	11.1	17.4
$f^o = 20\%$	4.1	7.1	12.6
$f^o = 30\%$	2.9	5.2	10.0
$f^o = 50\%$	1.8	3.4	7.1

While using logarithm concentration as metric variables yield better emission estimates than using the concentrations, the results in Table 3 are ap-

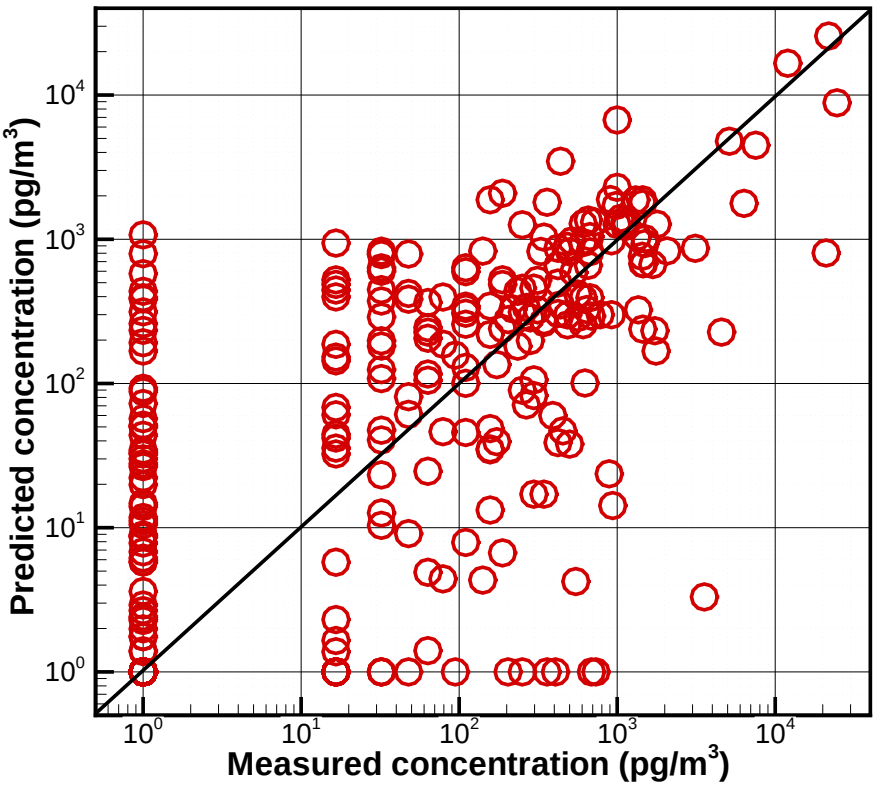

Figure 2: Comparison between the predicted and measured concentrations for Release 2 during the CAPTEX experiment. In the HYSPLIT simulation, at the exact release location, an emission rate of 67 kg/hr was applied from 17Z to 20Z on September 25, 1983. A constant 1 pg/m^3 is added to both predicted and measured concentrations to allow logarithm calculation.

Table 3: Emission strength of release 2 that minimizes $\mathcal{F}$ for different observational errors, defined as $\epsilon = f^o \times c_m + a^o$. Logarithm concentration is chosen as the metric variable, i.e. $(c_m^h - c_m^o)$ in Equation 1 is replaced with $ln(c_m^h) - ln(c_m^o)$.

Emission (kg/hr)	a^o =10 pg/m^3	a^o =20 pg/m^3	a^o =50 pg/m^3
$f^o = 10\%$	115.2	119.8	124.7
$f^o = 20\%$	106.3	112.9	119.8
$f^o = 30\%$	101.2	108.5	116.3
$f^o = 50\%$	94.4	101.2	109.6

parently systematically overestimated, comparing to the systematically underestimated results in Table 2. In addition, the f^o and a^o combinations associated with the best emission estimates in Tables 2 and 3 appear to go in opposite directions.

3.2. Recovering emission strength with model uncertainty

To consider the model uncertainties in a simplified way, ϵ^2 will be formulated as

$$\epsilon_m^2 = (f^o \times c_m^o + a^o)^2 + (f^h \times c_m^h + a^h)^2 \tag{3}$$

As a^o and a^h affect the ϵ^2 in a similar way, the representative errors caused by comparing the measurements with the predicted concentrations averaged in a grid can be included in either $(a^h)^2$ or $(a^o)^2$.

With logarithm concentration as the metric variable, $(\epsilon_m^{ln(c)})^2$ is comprised of two parts, as

$$(\epsilon_m^{ln(c)})^2 = [ln(1 + f^o + \frac{a^o}{c_m^o})]^2 + [ln(1 + f^h + \frac{a^h}{c_m^h})]^2 \tag{4}$$

Note that a constant small number 0.001 pg/m^3 is added to denominators c_m^o and c_m^h to avoid dividing by zero.

Using concentrations and logarithm concentration as metric variable, respectively, Tables 4 and 5 show the emission strength estimates with different f^h and a^h, while keeping $f^o = 20\%$, a^o =20 pg/m^3. It should be noted that the model uncertainties are not equivalent to model errors. Although dispersion model simulations can have large errors due to various reasons including the source term uncertainties, the model uncertainties are used to indicate that the model is not perfect even with the "optimal" model parameters.

Similar to weak constraint applied in operational 4D-Var data assimilation systems [55, 47], introducing model uncertainties is mainly intended to relax the model constraint for imperfect models. Here the f^h and a^h parameters are given similar ranges as those given to the observational uncertainty parameters.

When concentrations were used as metric variables, the emission strength estimates with model uncertainties considered were improved over those without model uncertainties. The estimates of emission strength generally increases with the model uncertainty, either through a^h or f^h except for $f^h = 50\%$, when the q estimates slowly decreases with a^h. The relationships between a^h versus q in Table 4 and a^o versus q in Table 2 are similar. When $f^h = 0\%$, $a^h = 10$, 20, and 50 pg/m^3 while a^o=20 pg/m^3, the q estimates, 7.7, 9.1, and 13.6 kg/hr, are inline with the results shown in Table 2, where $q = 7.1$ kg/hr for a^o=20 pg/m^3 and $q = 12.6$ kg/hr for a^o=50 pg/m^3. However, the trend of how q estimates change with f^h is opposite to how q estimates change with f^o. Table 4 shows that the emission strength increases with the model uncertainty factor f^h. With $f^h = 20\%$, the release estimates of 48.5, 50.4, and 53.5 kg/hr are all within 30% of the actual release rate of 67 kg/hr. Instead of underestimation shown in Table 2, the release estimates are actually overestimated when $f^h = 50\%$ is assumed.

With logarithm concentration as the metric variable, larger a^h or f^h results in slightly smaller q estimates. While how q estimates change with f_h is similar as how they change with f_a, how q estimates change with a^h is opposite to how q estimates change with a^o. Equation 4 shows that f_o and f_h affect $(\epsilon_m^{ln(c)})^2$ in a simple monotonic way, while the effect of a_m^h is complicated as it is divided by the c_m^h value that varies with the source terms. Table 5 shows that the emission strength are no longer overestimated as those in Table 3. In fact, all cases show slight to moderate underestimation, with the worst results being $q = 42.6$ kg/hr when $f^h = 50\%$ and a^h =50 pg/m^3. It should be noted that when concentrations were used as metric variables, $f^h = 50\%$ and a^h =50 pg/m^3 yield the best release estimate of 66.6 kg/hr. Another aspect of using logarithm concentrations as metric variables is that the range of the release estimates are not as large as those using concentrations as metric variables.

3.3. Cost function normalization

Without model uncertainties, the weighting terms for each model-observation pair do not change with emission estimates. When ϵ_m^2 and $(\epsilon_m^{ln(c)})^2$ are for-

Table 4: Emission strength of release 2 that minimizes $\mathcal{F}$ for different f^h and a^h. Concentration is taken as the metric variable. $\epsilon^2 = (f^o \times c^o + a^o)^2 + (f^h \times c^h + a^h)^2$. $f^o = 20\%$, a^o =20 pg/m^3.

Emission (kg/hr)	a^h =10 pg/m^3	a^h =20 pg/m^3	a^h =50 pg/m^3
$f^h = 0$	7.7	9.1	13.6
$f^h = 10\%$	15.9	22.1	32.9
$f^h = 20\%$	48.5	50.4	53.5
$f^h = 50\%$	114.0	111.8	104.3

Table 5: Emission strength of release 2 that minimizes $\mathcal{F}$ for different f^h and a^h. Logarithm concentration is taken as the metric variable. $\epsilon^2 = (f^o \times c^o + a^o)^2 + (f^h \times c^h + a^h)^2$. $f^o = 20\%$, a^o =20 pg/m^3.

Emission (kg/hr)	a^h =10 pg/m^3	a^h =20 pg/m^3	a^h =50 pg/m^3
$f^h = 0$	64.7	58.5	53.5
$f^h = 10\%$	61.5	55.7	49.4
$f^h = 20\%$	58.5	53.0	46.6
$f^h = 50\%$	55.1	49.4	42.6

mulated as in Equations 3 and 4, respectively, they change with emission estimates. When logarithm concentrations are used as metric variables, complication is found to be associated with the fact the weighting terms vary with emission estimates. Figure 3 shows the cost function as a function of source strength when $(\epsilon_m^{ln(c)})^2$ is defined as in Equation 4, with $f_h = 0$, a^h =50 pg/m^3, $f_o = 10\%$, a^o =20 pg/m^3. Before introducing cost function normalization, a global minimal cost function appears when release strength approaches zero while a local minimal cost function exists at 56.8 kg/hr. Several such situations were found when $a^h = 50$ pg/m^3 and when f_h is 0 or 10%, while both f_o and a^o are relatively small. The smaller cost function when release strength approaches zero is due to the increasing $(\epsilon_m^{ln(c)})^2$ in Equation 4 as c_m^h gets smaller. While the model-observation differences are not smaller for lower release strength, the drastic change of $(\epsilon_m^{ln(c)})^2$ when $a^h = 50$ pg/m^3 and f_h is 0 or 10% results in smaller cost function with decreasing source strength. To avoid having zero source as a global minimizer in such situations, the total weighted mismatch between model simulation and observations are normalized by the total weights when $q_{ij} = q_{ij}^b$, as shown

in Equation 5.

$$\mathcal{F} = \frac{1}{2}\sum_{i=1}^{M}\sum_{j=1}^{N}\frac{(q_{ij}-q_{ij}^{b})^2}{\sigma_{ij}^2} + \frac{1}{2}\sum_{m=1}^{M}\frac{(c_m^h - c_m^o)^2}{\epsilon_m^2} \times \frac{\sum_{m=1}^{M}\frac{1}{\epsilon_m^{b\,2}}}{\sum_{m=1}^{M}\frac{1}{\epsilon_m^2}} + \frac{c_{sm}}{2}\cdot\sum_{i=2}^{N-1}[\frac{(q_{i-1,j}-q_{i-1,j}^{b}) - 2\cdot(q_{ij}-q_{ij}^{b}) + (q_{i+1,j}-q_{i+1,j}^{b})}{q_c}]^2 \quad (5)$$

Figure 3 shows that the cost function has the minimum at q=67.3 kg/hr after normalization. Note that the dramatic difference of the cost function magnitude before and after the normalization is due to the extreme small value of $\sum_{m=1}\frac{1}{\epsilon_m^{b\,2}}$ calculated at $q_b = 0$. A constant small number 0.001 pg/m^3 is added to denominators c_m^o and c_m^h to avoid dividing by zero when $(\epsilon_m^{ln(c)})^2$ is calculated as defined in Equation 4. Tables 6 and 7 show the emission strength estimates after cost function normalization with different f^h and a^h, while keeping $f^o = 20\%$, a^o =20 pg/m^3, using concentrations and logarithm concentrations as metric variables, respectively. Note that $f_o = 20\%$ was chosen for the cases listed in Table 7, while $f_o = 10\%$ was chosen in Figure 3 to illustrate the potential problem. How estimate changes with f^h and a^h are similar to those in Tables 4 and 5. The estimates are generally closer to the actual release than those obtained without the cost function normalization.

When using concentrations as metric variables, the emission strength estimates with $f^h = 50\%$ are 64.7, 64.7, and 65.3 kg/hr for a^h=10, 20, 50 pg/m^3, respectively. They are all within 5% of the actual release. However, f^h less than or equal to 20% results in significant underestimation. When using logarithm concentrations as metric variables, the source term estimates are not very sensitive to f^h and a^h values and the results listed in Table 5 are all withing 20% of the actual release. Among those estimates, 67.3 kg/hr when $f^h = 10\%$ and a^h=10 pg/m^3 is almost identical to the actual release.

3.4. Ensemble

Ngan and Stein [34] simulated CAPTEX releases using a variety of planetary boundary layer (PBL) schemes. In their configuration, WRF version 3.5.1 was used with 27-km grid spacing and 33 vertical layers. North American Regional Reanalysis (NARR) [32] data set was used for the initial conditions and lateral boundary conditions. The WRF model was initialized

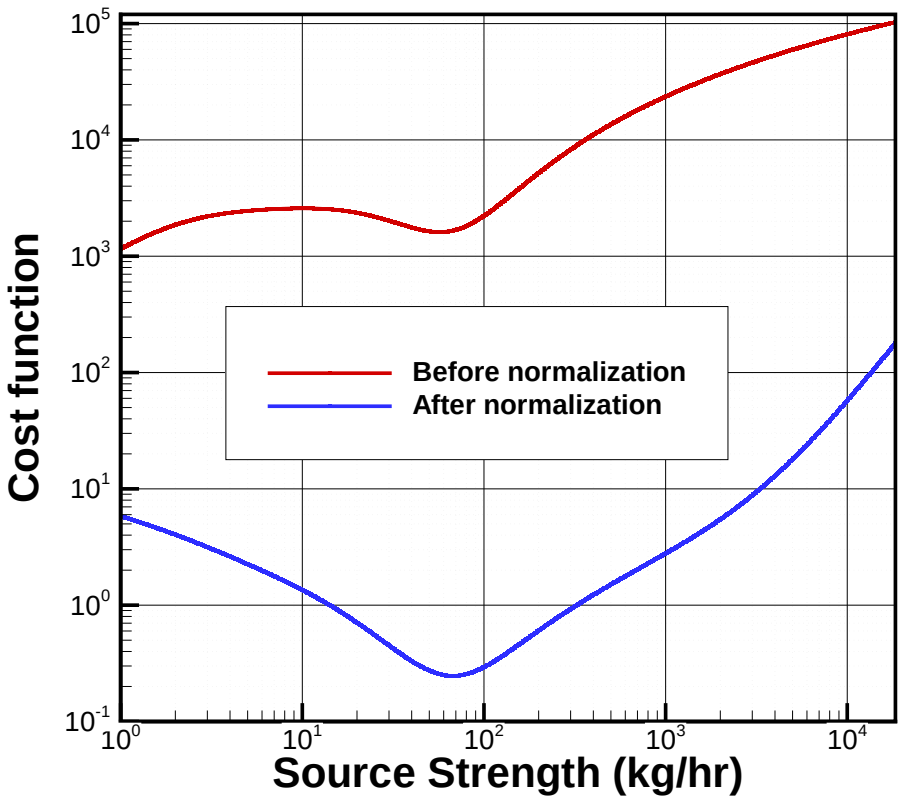

Figure 3: Cost function as a function of source strength when $(\epsilon_m^{ln(c)})^2$ is defined as in Equation4 before and after cost function normalization, with $f_h = 0$, a^h =50 pg/m^3, $f_o = 10\%$, a^o =20 pg/m^3.

Table 6: Emission strength of release 2 that minimizes normalized $\mathcal{F}$ defined in Equation 3 for different f^h and a^h. Concentration is taken as the metric variable. $\epsilon^2 = (f^o \times c^o + a^o)^2 + (f^h \times c^h + a^h)^2$. $f^o = 20\%$, a^o =20 pg/m^3.

Emission (kg/hr)	a^h =10 pg/m^3	a^h =20 pg/m^3	a^h =50 pg/m^3
$f^h = 0$	7.7	9.1	13.6
$f^h = 10\%$	10.9	15.1	26.4
$f^h = 20\%$	32.9	35.6	41.3
$f^h = 50\%$	64.7	64.7	65.3

Table 7: Emission strength of release 2 that minimizes normalized $\mathcal{F}$ defined in Equation 3 for different f^h and a^h. Logarithm concentration is taken as the metric variable. $\epsilon^2 = (f^o \times c^o + a^o)^2 + (f^h \times c^h + a^h)^2$. $f^o = 20\%$, a^o =20 pg/m^3.

Emission (kg/hr)	a^h =10 pg/m^3	a^h =20 pg/m^3	a^h =50 pg/m^3
$f^h = 0$	69.3	64.0	62.1
$f^h = 10\%$	67.3	63.4	60.9
$f^h = 20\%$	65.3	61.5	59.1
$f^h = 50\%$	61.5	58.0	55.1

every day at 0600 UTC, and the first 18 hours of spin-up time in the 42-hour simulation were discarded. The PBL schemes used to create the WRF ensemble were the Yonsei University [25, YSU]), Mellor-Yamada-Janjic [27, MYJ], Quasi-Normal Scale Elimination [37, QNSE], MYNN 2.5 level TKE [33, MYNN], ACM2 [38, ACM2], Bougeault and Lacarrere [7, BouLac], University of Washington [8, UW], Total energy mass flux [2, TEMF], and Grenier Bretherton MaCaa [21, GBM] schemes. Nine simulations were conducted with the PBL schemes and their associated surface layer schemes, except for the YSU, BouLac, UW, and GBM cases in which the MM5 Monin-Obukhov surface scheme was applied. The land-surface model was Noah land-surface model [11], except ACM2 case in which Pleim-Xiu land-surface model was used.

An individual TCM is generated using each of the nine simulations. The nine TCMs can be used to estimate the emission strengths independently following the same procedure as described previously. Tables 8 and 9 show the 3rd (25th percentile), 5th (median), and 7th (75th percentile) emission strength of the nine simulations of release 2 that minimizes the normalized $\mathcal{F}$

defined in Equation 3 with different f^h and a^h, while keeping $f^o = 20\%$, a^o =20 pg/m^3, using concentrations and logarithm concentration as metric variable, respectively. The 25th percentile and 75th percentile values are mostly within 5% of the median estimates. While the median estimates show the same trends with f^h and a^h as the results in Tables 6 and 7, the median estimates are significantly larger due to the meteorological model differences. Apparently the differences among the simulations with different PBL schemes are smaller than the differences between the ensemble simulations here and the simulation used in the earlier sections. This suggests that uncertainties of the emission strength are probably larger than the ranges indicated by the 25th and 75th percentile values. The results using logarithm concentrations as metric variables are quite robust with the listed model uncertainty parameters. However, the estimates using concentrations as metric variables are very sensitive with f^h and a^h. This is consistent with results shown in Section 3.2.

Instead of using each individual TCM generated from nine simulations independently, the nine TCMs can be combined into one matrix by taking the median or average of transfer coefficients. The combined TCM can then be used to estimate the source terms and the results are listed in Tables 10 and 11. It is found that the emission estimate using the median transfer coefficients of the nine TCMs are very close to the median of the nine estimates using the nine simulations individually. For the cases with logarithm concentrations as metric variables, the emission estimates using the median value of the nine TCMs are all within 3.1% of that using the median value of the nine TCMs. For the cases with concentrations as metric variables, the average relative differences are 6.4%, with the maximum relative difference being 10.8% when $f^h = 10\%$ and a^h=50 pg/m^3. Combining the TCMs by taking the median value generates slightly better results than combining the TCMs by taking the average value does.

Similar to what was found in earlier sections and also in Chai et al. [10], the cases having logarithm concentrations as metric variables generally yield better results than those having concentrations as metric variables. It is probably due to the large range of the concentrations. When having concentrations as metric variables, certain model uncertainty parameters yield good source terms, but the estimates are quite sensitive to the choices of the model uncertainty parameters. However, it is not easy to find such model uncertainty parameters that would yield satisfactory results for applications when the actual releases are indeed unknown. The results here and in the

previous sections show that the estimates when having logarithm concentrations as metric variables are quite robust for a reasonable range of model uncertainty parameters. For these two reasons, logarithm concentrations are chosen as metric variables for the later tests.

Table 8: The 3rd (25th percentile), 5th (median), and 7th (75th percentile) emission strength of nine simulations of release 2 that minimizes the normalized $\mathcal{F}$ defined in Equation 3 Concentration is taken as the metric variable. $\epsilon^2 = (f^o \times c^o + a^o)^2 + (f^h \times c^h + a^h)^2$. $f^o = 20\%$, a^o =20 pg/m^3.

Emission (kg/hr)	a^h =10 pg/m^3	a^h =20 pg/m^3	a^h =50 pg/m^3
$f^h = 0$	6.0, 7.0, 7.2	7.4, 8.8, 8.8	13.4, 15.1, 15.3
$f^h = 10\%$	20.0, 21.0, 21.9	23.9, 26.1, 27.2	33.2, 35.2, 37.4
$f^h = 20\%$	48.5, 49.9, 59.1	53.0, 54.6, 62.8	58.5, 62.8, 68.6
$f^h = 50\%$	191, 205, 274	186, 197, 258	158, 168, 207

Table 9: The 3rd (25th percentile), 5th (median), and 7th (75th percentile) emission strength of nine simulations of release 2 that minimizes normalized $\mathcal{F}$ defined in Equation 3 for different f^h and a^h. Logarithm concentration is taken as the metric variable. $\epsilon^2 = (f^o \times c^o + a^o)^2 + (f^h \times c^h + a^h)^2$. $f^o = 20\%$, a^o =20 pg/m^3.

Emission (kg/hr)	a^h =10 pg/m^3	a^h =20 pg/m^3	a^h =50 pg/m^3
$f^h = 0$	102, 106, 113	93.4, 100, 105	83.8, 88.9, 97.2
$f^h = 10\%$	97.2, 102, 108	88.9, 96.3, 101	80.5, 85.4, 94.4
$f^h = 20\%$	93.4, 98.2, 105	86.3, 92.5, 98.2	78.1, 82.9, 91.6
$f^h = 50\%$	88.9, 93.4, 101	82.9, 88.0, 94.4	75.8, 81.3, 87.2

3.5. Source location and other releases

In addition to the source strength, the source location and its temporal variation can be retrieved with adequate accuracy using the HYSPLIT inverse system described here if there are sufficient observational information available. For instance, Chai et al. [10] estimated 99 6-hr emission rates of the radionuclide Cesium-137 from the Fukushima nuclear accident using 1296 daily average air concentration measured at 115 stations around the globe. Here the system's capability to locate a single source location will be tested using a straightforward approach. The release time is assumed known, but

Table 10: Emission strength estimates by using average and median value of nine simulations for release 2. The cost function is normalized $\mathcal{F}$ as in Equation 3. Concentration is taken as the metric variable. $\epsilon^2 = (f^o \times c^o + a^o)^2 + (f^h \times c^h + a^h)^2$. $f^o = 20\%$, a^o =20 pg/m^3.

Emission (kg/hr)	a^h =10 pg/m^3	a^h =20 pg/m^3	a^h =50 pg/m^3
$f^h = 0$	7.2, 7.5	8.9, 9.1	15.6, 15.9
$f^h = 10\%$	22.3, 23.4	22.2, 28.0	37.0, 37.0
$f^h = 20\%$	55.1, 53.0	59.7, 58.0	66.6, 64.7
$f^h = 50\%$	213, 227	205, 213	178, 177

Table 11: Emission strength estimates by using average and median value of nine simulations for release 2. The cost function is normalized $\mathcal{F}$ as in Equation 3. Logarithm concentration is taken as the metric variable. $\epsilon^2 = (f^o \times c^o + a^o)^2 + (f^h \times c^h + a^h)^2$. $f^o = 20\%$, a^o =20 pg/m^3.

Emission (kg/hr)	a^h =10 pg/m^3	a^h =20 pg/m^3	a^h =50 pg/m^3
$f^h = 0$	115, 108	105, 100	95.3, 90.7
$f^h = 10\%$	110, 103	100, 95.3	91.6, 87.2
$f^h = 20\%$	105, 100	97.2, 92.5	88.9, 85.4
$f^h = 50\%$	100, 96.3	93.4, 88.9	86.3, 82.1

its location and strength are left to be determined. A region of suspect is first gridded at certain spatial resolution to form a limited number of candidate source locations. An optimal strength is then found at each candidate source location following the method described earlier. The location that results in the best match between the predicted and the observed concentrations is considered as the likely source location.

In the following tests, a 11×11 grid with 0.2° resolution in both longitude and latitude directions is used to generate 121 candidate source locations. They are centered at (40.0°N, 84.5°W) for releases 1-4, and centered at (46.6°N, 80.8°W) for releases 5 and 7. Using the normalized $\mathcal{F}$ defined in Equation 3 and assuming $f^o = 20\%$, a^o =20 pg/m^3, $f^h = 20\%$, a^h =20 pg/m^3, an minimal cost function associated with an optimal release strength can be found at each location. Figure 4 shows the 121 candidate locations and their respective minimal cost function values for release 2. No candidate locations are chosen to collocate with the actual source location which will

be unknown for the future applications that need to locate the sources. A global minimal point is found at (39.8°N, 84.5°), with $\mathcal{F} = 3.14$ achieved when q=48.5 kg/hr. This grid point is taken as the estimated source location and it is 26.4 km away from the actual release site (39.90°N, 84.22°W). The neighboring location (39.8°N, 84.3°W) which is the closest to the actual release site yields a slightly larger $\mathcal{F} = 3.17$ with a release rate of 60.9 kg/hr. If the exact source location is known as in the tests presented earlier, the cost function $\mathcal{F}$ reaches 1.59 at its minimal point when $q = 61.5$ kg/hr. Apparently, compared with those cases when the release strength is the only unknown, finding both the source location and its strength with the same amount of observations is expected to be more difficult. Note that the smaller normalized F values in Figure 3 are for a case with different observation and model uncertainty parameters, where $f^o = 10\%$, a^o =20 pg/m^3, $f^h = 0\%$, and a^h =50 pg/m^3.

Table 12 lists the source location and strength estimations for all releases following the same procedure as release 2 described here, where the uncertainty parameters are $f^o = 20\%$, a^o =20 pg/m^3, $f^h = 20\%$, and a^h =20 pg/m^3. Releases 1 and 4 have the minimal cost function $\mathcal{F}_{min}$ occur at the north boundary and the west boundary, respectively. In such scenarios, it might be necessary to expand the suspected source region for the future applications to find the source locations. However, if source locations are known to reside in the suspected region, the sources can definitely be near the boundaries. In such cases, the point with $\mathcal{F}_{min}$ should be considered as the estimated source location. Releases 3, 5, and 7 have its $\mathcal{F}_{min}$ occurred at inner grid points, similar to release 2 shown in Figure 4. None of the closest candidate source locations yield the best match between model simulation and observations quantified by the cost function $\mathcal{F}$. Among the six releases, the estimated source location for release 2 is the closest to its actual release site, with a distance of 26.4 km.

The release rates obtained along with the likely source locations are underestimated by a factor of 3 for release 1, and overestimated by a factor of 3 for releases 4 and 7, although the estimates for releases 2, 3, and 5 are much better, with relative errors as -27.6%, -5.4%, and 21.5%, respectively. Table 12 also lists the release rates estimated with the exact source location assumed known. These estimates for all releases are within a factor of two compared with the actual release rates and the largest relative error is 53.3% for release 1. Either with the source location known or unknown, release 2 has the best emission estimates among the six releases, because the HYS-

PLIT forward model also has the best performance for the same release [23]. The significant model errors when simulating the transport and dispersion even with the exact source terms are mostly caused by the meteorological uncertainties while the HYSPLIT physical schemes and parameters, as well as the numerical discretization also contribute.

The meteorological field and the observations are the two major inputs to the current inverse modeling. As discussed above, better model performance of release 2 helps to lead to better inverse results than the other releases. However, it is impossible to eliminate the model uncertainties. In practice, ensemble runs can be used to quantify the uncertainties and reduce the model errors by taking the average or median values of the ensemble runs. On the other hand, increasing the number of observations is effective to improve the inverse modeling results and reduce the result uncertainty. In principle, when the release strength is the only value to be determined, each measurement within the predicted plume can provide an independent estimate. However, relying on a single observation to estimate the strength is problematic since a particular model output can be very different from the observation and thus leading to an erroneous estimation of the source strength when used in isolation. For instance, although the HYSPLIT predictions of the release 2 with exact source terms are very good, compared with individual measurements, it has severe underestimation, 0.77 pg/m^3 predicted versus 686 pg/m^3 measured, as well as significant overestimation, 2033 pg/m^3 predicted versus 31.2 pg/m^3 measured. Therefore, similar to a regression technique, increasing the sampling number can improve the final results, as shown by the very good source term estimation for release 2 when using all the available measurements. Also note that the samples outside predicted plumes do not contribute to the inverse modeling. Table 1 lists the total measurement counts for each release, but the number of measurements actually contributing to the inverse modeling are those inside the HYSPLIT plumes, including those with zero or background concentrations. The number of such effective measurements inside the plumes generated by HYSPLIT with unit emission rate from the exact source location and time period are reduced to 148, 237, 211, 68, 46, and 53, for releases 1–5, and 7, respectively. The largest number of effective measurements, 237, of release 2, also indicates the best performance of the HYSPLIT simulation among those of the six releases. The effective measurements will change when source location or timing is changed. The measurements that is not active in determining the source strength with known source location and timing may be effective to

locate the source locations.

Table 12: The source location (latitude, longitude) and release rate q_{min} identified by the minimal normalized cost function $\mathcal{F}_{min}$ for each CAPTEX release. A total of 121 candidate locations are prescribed with 0.2° resolution in both longitude and latitude directions, centered at (40.0°N, 84.5°W) for releases 1-4, and at (46.6°N, 80.8°W) for releases 5 and 7. Δ is the distance between the point with $\mathcal{F}_{min}$ and the actual release site. q' is the estimated release rate by assuming that the actual release location is known. For all the cases, $f^o = 20\%$, a^o =20 pg/m^3, $f^h = 20\%$, and a^h =20 pg/m^3.

#	Source location (latitude, longitude)		Δ(km)	Release rate (kg/hr)		
	Actual	Estimated		Actual	q_{min}	q'
1	39.80°, -84.05°	41.0°,-83.9°	134.2	69.3	23.9	106.3
2	39.90°, -84.22°	39.8°,-84.5°	26.4	67.0	48.5	61.5
3	39.90°, -84.22°	40.8°,-85.3°	135.8	67.0	63.4	41.7
4	39.90°, -84.22°	40.2°,-85.5°	114.1	66.3	185.7	75.1
5	46.62°, -80.78°	46.2°,-81.0°	49.7	60.0	72.9	42.6
7	46.62°, -80.78°	47.4°,-81.2°	92.5	61.0	201.0	66.0

4. Summary

An HYSPLIT inverse system developed to estimate the source term parameters was evaluated using the Cross Appalachian Tracer Experiment (CAPTEX) data collected from six controlled releases. In the HYSPLIT inverse system, a cost function is used to measure the differences between model predictions and observations weighted by the observational uncertainties. Inverse modeling tests with various observational uncertainties show that using concentration differences results in severe underestimation while using logarithm concentrations differences results in overestimation. Introducing model uncertainty terms improves inverse results for both choices of the metric variables in the cost function. It is also found that cost function normalization can avoid spurious minimal source terms when using logarithm concentrations as metric variables. The inverse tests show that having logarithm concentrations as metric variables generally yields better results than having concentrations as metric variables. The estimates having logarithm concentrations as metric variables are robust for a reasonable range of model uncertainty parameters. Such conclusions are further confirmed with nine

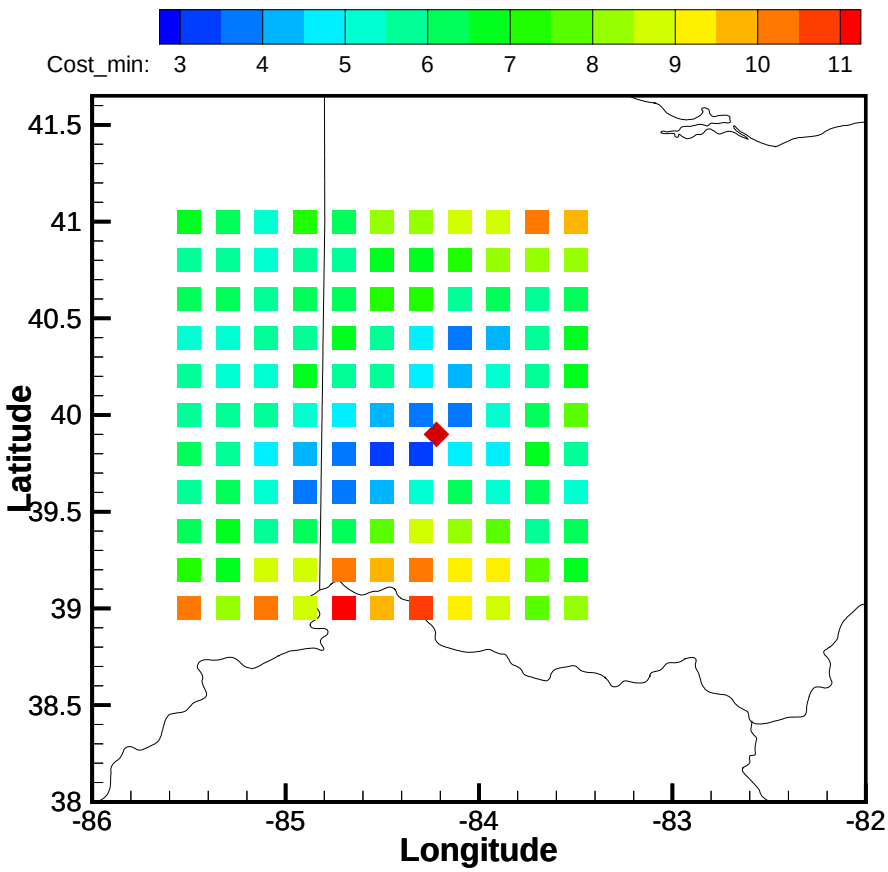

Figure 4: Distribution of 121 candidate source locations for release 2. The minimal cost function at each location associated with an optimal release strength is indicated by color. The cost function is calculated using Equation 3 where f^o = 20%, a^o =20 pg/m^3, f^h = 20%, and a^h =20 pg/m^3. The actual source location , Dayton, Ohio, U.S., is shown as a red diamond.

ensemble runs where meteorological fields were generated using a different version of WRF meteorological model with varying PBL schemes.

With a fixed set of observational and model uncertainty parameters, the inverse method with logarithm concentrations as metric variables is then applied to all the six releases. The emission rates are well recovered with the largest relative error as 53.3% for release 1. The system is later tested for its capability to locate a single source location as well as its source strength. The location and strength that result in the best match between the predicted and the observed concentrations are considered as the inverse results. The estimated location is close to the actual release site for release 2 of which the forward HYSPLIT model has the best performance. The strength estimation is within a factor of 3 for all releases.

Acknowledgments

This study was supported by NOAA grant NA09NES4400006 (Cooperative Institute for Climate and Satellites-CICS) at the NOAA Air Resources Laboratory in collaboration with the University of Maryland.

References

[1] Achim, P., Monfort, M., Le Petit, G., Gross, P., Douysset, G., Taffary, T., Blanchard, X., Moulin, C., MAR 2014. Analysis of Radionuclide Releases from the Fukushima Dai-ichi Nuclear Power Plant Accident Part II. Pure Appl. Geophys. 171 (3-5), 645–667.

[2] Angevine, W. M., Jiang, H., Mauritsen, T., 2010. Performance of an eddy diffusivity-mass flux scheme for shallow cumulus boundary layers. Monthly Weather Review 138 (7), 2895–2912.

[3] Bieringer, P. E., Young, G. S., Rodriguez, L. M., Annunzio, A. J., Vandenberghe, F., Haupt, S. E., 2017. Paradigms and commonalities in atmospheric source term estimation methods. Atmos. Environ. 156, 102 – 112.

[4] Bocquet, M., 2005. Reconstruction of an atmospheric tracer source using the principle of maximum entropy. II: Applications. Quart. J. Roy. Meteor. Soc. 131 (610, B), 2209–2223.

[5] Bocquet, M., 2007. High-resolution reconstruction of a tracer dispersion event: application to ETEX. Quart. J. Roy. Meteor. Soc. 133 (625, B), 1013–1026.

[6] Bocquet, M., 2008. Inverse modelling of atmospheric tracers: non-Gaussian methods and second-order sensitivity analysis. Nonlinear Processes in Geophysics 15 (1), 127–143.

[7] Bougeault, P., Lacarrère, P., AUG 1989. Parameterization of orography-induced turbulence in a mesobeta-scale model. Monthly Weather Review 117 (8), 1872–1890.

[8] Bretherton, C. S., Park, S., 2009. A new moist turbulence parameterization in the community atmosphere model. J. of Climate 22 (12), 3422–3448.

[9] Chai, T., Crawford, A., Stunder, B., Pavolonis, M. J., Draxler, R., Stein, A., 2017. Improving volcanic ash predictions with the HYSPLIT dispersion model by assimilating MODIS satellite retrievals. Atmos. Chem. Phys. 17 (4), 2865–2879.

[10] Chai, T., Draxler, R., Stein, A., 2015. Source term estimation using air concentration measurements and a Lagrangian dispersion model - Experiments with pseudo and real cesium-137 observations from the Fukushima nuclear accident. Atmos. Environ. 106, 241–251.

[11] Chen, F., Dudhia, J., 2001. Coupling an advanced land surface-hydrology model with the Penn State-NCAR MM5 modeling system. Part I: Model implementation and sensitivity. Monthly Weather Review 129 (4), 569–585.

[12] Chino, M., Nakayama, H., Nagai, H., Terada, H., Katata, G., Yamazawa, H., JUL 2011. Preliminary Estimation of Release Amounts of I-131 and Cs-137 Accidentally Discharged from the Fukushima Daiichi Nuclear Power Plant into the Atmosphere. J. Nucl. Sci. Technol. 48 (7), 1129–1134.

[13] Daley, R., 1991. Atmospheric Data Analysis. Cambridge University Press, Cambridge.

[14] Draxler, R., 1987. Sensitivity of a trajectory model to the spatial and temporal resolution of the meteorological data during CAPTEX. J. Climate Appl. Meteor. 26 (11), 1577–1588.

[15] Draxler, R., Dietz, R., Lagomarsino, R., Start, G., 1991. Across North-America tracer experiment (ANATEX) - sampling and analysis. Atmos. Environ. 25 (12), 2815–2836.

[16] Draxler, R., Hess, G., December 1997. Description of the HYSPLIT_4 modeling system. Tech. Rep. NOAA Technical Memo ERL ARL-224, National Oceanic and Atmospheric Administration, Air Resources Laboratory, Silver Spring, Maryland, USA.

[17] Draxler, R., Hess, G., December 1998. An overview of the HYSPLIT_4 modeling system for trajectories, dispersion and deposition. Aust. Meteor. Mag. 47 (4), 295–308.

[18] Draxler, R. R., Rolph, G. D., 2012. Evaluation of the Transfer Coefficient Matrix (TCM) approach to model the atmospheric radionuclide air concentrations from Fukushima. J. of Geophys. Res. 117, D05107.

[19] Fay, B., Glaab, H., Jacobsen, I., Schrodin, R., 1995. Evaluation of Eulerian and llagrangian atmospheric transport models at the Deutscher-Wetterdienst using ANATEX surface tracer data. Atmos. Environ. 29 (18), 2485–2497.

[20] Ferber, G., Heffter, J., Draxler, R., Lagomarisino, R., Thomas, F., January 1986. Cross-Appalachian Tracer Experiment (CAPTEX '83) final report. Tech. Rep. NOAA Technical Memorandum ERL ARL-142, National Oceanic and Atmospheric Administration, Silver Spring, Maryland, USA, available online at https://www.arl.noaa.gov/documents/reports/arl-142.pdf.

[21] Grenier, H., Bretherton, C., 2001. A moist PBL parameterization for large-scale models and its application to subtropical cloud-topped marine boundary layers. Monthly Weather Review 129 (3), 357–377.

[22] Hanna, S., Egan, B., Purdum, J., 2001. Evaluation of the ADMS, AERMOD, and ISC3 dispersion models with the OPTEX, Duke Forest, Kincaid, Indianapolis and Lovett field datasets. International Journal of Environment and Pollution 16 (1-6, SI), 301–314.

[23] Hegarty, J., Draxler, R. R., Stein, A. F., Brioude, J., Mountain, M., Eluszkiewicz, J., Nehrkorn, T., Ngan, F., Andrews, A., 2013. Evaluation of Lagrangian Particle Dispersion Models with Measurements from Controlled Tracer Releases. J. Appl. Meteor. Climatol. 52 (12), 2623–2637.

[24] Hirao, S., Yamazawa, H., Nagae, T., FEB 2013. Estimation of release rate of iodine-131 and cesium-137 from the Fukushima Daiichi nuclear power plant. J. Nucl. Sci. Technol. 50 (2), 139–147.

[25] Hong, S.-Y., Noh, Y., Dudhia, J., 2006. A new vertical diffusion package with an explicit treatment of entrainment processes. Monthly Weather Review 134 (9), 2318–2341.

[26] Hutchinson, M., Oh, H., Chen, W.-H., 2017. A review of source term estimation methods for atmospheric dispersion events using static or mobile sensors. Information Fusion 36, 130–148.

[27] JANJIC, Z., 1994. The step-mountain eta coordinate model - further developments of the convection, viscous sublayer, and turbulence closure schemes. Monthly Weather Review 122 (5), 927–945.

[28] Katata, G., Chino, M., Kobayashi, T., Terada, H., Ota, M., Nagai, H., Kajino, M., Draxler, R., Hort, M. C., Malo, A., Torii, T., Sanada, Y., 2014. Detailed source term estimation of the atmospheric release for the Fukushima Daiichi nuclear power station accident by coupling simulations of atmospheric dispersion model with improved deposition scheme and oceanic dispersion model. Atmos. Chem. Phys. Discuss. 14 (10), 14725–14832, available online at http://www.atmos-chem-phys-discuss.net/14/14725/2014/.

[29] Katata, G., Ota, M., Terada, H., Chino, M., Nagai, H., JUL 2012. Atmospheric discharge and dispersion of radionuclides during the Fukushima Dai-ichi Nuclear Power Plant accident. Part I: Source term estimation and local-scale atmospheric dispersion in early phase of the accident. J. Environ. Radioact. 109, 103–113.

[30] Kobayashi, T., Nagai, H., Chino, M., Kawamura, H., 2013. Source term estimation of atmospheric release due to the Fukushima Dai-ichi Nuclear Power Plant accident by atmospheric and oceanic dispersion simulations. J. Nucl. Sci. Technol. 50 (3), 255–264.

[31] Lin, C.-L., Chai, T., Sun, J., 2002. On smoothness constraints for four-dimensional data assimilation. J. Comput. Physics 181, 430–453.

[32] Mesinger, F., DiMego, G., Kalnay, E., Mitchell, K., Shafran, P., Ebisuzaki, W., Jovic, D., Woollen, J., Rogers, E., Berbery, E., Ek, M., Fan, Y., Grumbine, R., Higgins, W., Li, H., Lin, Y., Manikin, G., Parrish, D., Shi, W., 2006. North American regional reanalysis. Bull. Amer. Meteorol. Soc. 87 (3), 343–360.

[33] Nakanishi, M., Niino, H., 2006. An improved Mellor-Yamada level-3 model: Its numerical stability and application to a regional prediction of advection fog. Bound.-Layer Meteorol. 119 (2), 397–407.

[34] Ngan, F., Stein, A., 2017. A Long-Term WRF Meteorological Archive for Dispersion Simulations: Application to Controlled Tracer Experiments. J. Appl. Meteor. Climatol. 56 (8), 2203–2220.

[35] Ngan, F., Stein, A., Draxler, R., 2015. Inline coupling of WRF-HYSPLIT: Model development and evaluation using tracer experiments. J. Appl. Meteor. Climatol. 54 (6), 1162–1176.

[36] Oza, R. B., Indumati, S. P., Puranik, V. D., Sharma, D. N., Ghosh, A. K., AUG 2013. Simplified approach for reconstructing the atmospheric source term for Fukushima Daiichi nuclear power plant accident using scanty meteorological data. Ann. Nucl. Energy 58, 95–101.

[37] Pergaud, J., Masson, V., Malardel, S., Couvreux, F., 2009. A parameterization of dry thermals and shallow cumuli for mesoscale numerical weather prediction. Bound.-Layer Meteorol. 132 (1), 83–106.

[38] Pleim, J. E., 2007. A combined local and nonlocal closure model for the atmospheric boundary layer. part I: Model description and testing. J. Appl. Meteor. Climatol. 46 (9), 1383–1395.

[39] Prata, A., Grant, I., 2001. Retrieval of microphysical and morphological properties of volcanic ash plumes from satellite data: Application to Mt Ruapehu, New Zealand. Quart. J. Roy. Meteor. Soc. 127 (576, B), 2153–2179.

[40] Rolph, G. D., Draxler, R. R., Stein, A. F., Taylor, A., Ruminski, M. G., Kondragunta, S., Zeng, J., Huang, H.-C., Manikin, G., Mcqueen, J. T., Davidson, P. M., 2009. Description and verification of the NOAA smoke forecasting system: the 2007 fire season. Weather and Forecasting 24 (2), 361–378.

[41] Saunier, O., Mathieu, A., Didier, D., Tombette, M., Quelo, D., Winiarek, V., Bocquet, M., 2013. An inverse modeling method to assess the source term of the Fukushima Nuclear Power Plant accident using gamma dose rate observations. Atmos. Chem. Phys. 13 (22), 11403–11421.

[42] Singh, S. K., Rani, R., 2014. A least-squares inversion technique for identification of a point release: Application to Fusion Field Trials 2007. Atmos. Environ. 92, 104–117.

[43] Singh, S. K., Turbelin, G., Issartel, J.-P., Kumar, P., Feiz, A. A., 2015. Reconstruction of an atmospheric tracer source in Fusion Field Trials: Analyzing resolution features. J. of Geophys. Res. 120 (12), 6192–6206.

[44] Stein, A. F., Draxler, R. R., Rolph, G. D., Stunder, B. J. B., Cohen, M. D., Ngan, F., 2015. NOAA's HYSPLIT atmospheric transport and dispersion modeling system. Bull. Amer. Meteorol. Soc. 96 (12), 2059–2077.

[45] Stohl, A., Seibert, P., Wotawa, G., Arnold, D., Burkhart, J. F., Eckhardt, S., Tapia, C., Vargas, A., Yasunari, T. J., 2012. Xenon-133 and caesium-137 releases into the atmosphere from the Fukushima Dai-ichi nuclear power plant: determination of the source term, atmospheric dispersion, and deposition. Atmos. Chem. Phys. 12 (5), 2313–2343.

[46] Terada, H., Katata, G., Chino, M., Nagai, H., OCT 2012. Atmospheric discharge and dispersion of radionuclides during the Fukushima Dai-ichi Nuclear Power Plant accident. Part II: verification of the source term and analysis of regional-scale atmospheric dispersion. J. Environ. Radioact. 112, 141–154.

[47] Tremolet, Y., 2006. Accounting for an imperfect model in 4D-Var. Quart. J. Roy. Meteor. Soc. 132 (621, B), 2483–2504.

[48] Van Dop, H., Addis, R., Fraser, G., Girardi, F., Graziani, G., Inoue, Y., Kelly, N., Klug, W., Kulmala, A., Nodop, K., Pretel, J., 1998. ETEX: A European tracer experiment; Observations, dispersion modelling and emergency response. Atmos. Environ. 32 (24), 4089–4094.

[49] Wen, S., Rose, W. I., 1994. Retrieval of sizes and total masses of particles in volcanic clouds using AVHRR bands 4 and 5. J. of Geophys. Res. 99 (D3), 5421–5431.

[50] Wilkins, K. L., Mackie, S., Watson, I. M., Webster, H. N., Thomson, D. J., Dacre, H. F., 2014. Data insertion in volcanic ash cloud forecasting. Ann Geophys 57.

[51] Wilkins, K. L., Watson, I. M., Kristiansen, N. I., Webster, H. N., Thomson, D. J., Dacre, H. F., Prata, A. J., 2016. Using data insertion with the NAME model to simulate the 8 May 2010 Eyjafjallajokull volcanic ash cloud. J. of Geophys. Res. 121 (1), 306–323.

[52] Winiarek, V., Bocquet, M., Duhanyan, N., Roustan, Y., Saunier, O., Mathieu, A., 2014. Estimation of the caesium-137 source term from the

Fukushima Daiichi nuclear power plant using a consistent joint assimilation of air concentration and deposition observations. Atmos. Environ. 82, 268–279.

[53] Winiarek, V., Bocquet, M., Saunier, O., Mathieu, A., 2012. Estimation of errors in the inverse modeling of accidental release of atmospheric pollutant: Application to the reconstruction of the cesium-137 and iodine-131 source terms from the Fukushima Daiichi power plant. J. Geophys. Res. - Atmos. 117, D05122.

[54] Zhu, C., Byrd, R. H., Lu, P., Nocedal, J., 1997. L-BFGS-B–fortran suroutines for large scale bound constrained optimization. ACM Trans. Math. Software 23 (4), 550–560.

[55] Zupanski, D., 1997. A general weak constraint applicable to operational 4DVAR data assimilation systems. Monthly Weather Review 125 (9), 2274–2292.